PHOTOGEOLOGIC ANALYSIS OF THE MAGELLAN STEREO VIEW OF SIX CORONAE

A.T.Basilevsky[1,2] and J.W.Head[2]. [1]Vernadsky Inst., Russian Academy of Sciences, Moscow 117975, Russia, abasilevsky@glasnet.ru; [2]Dept. Geol. Sci., Brown Univ., RI 02912 USA.

INTRODUCTION. The present study is one of efforts of many researches to progress in the stratigraphic context of local, regional, and global geology of coronae (see for example, [1-4,6-9]). This study is based on photogeologic analysis of several coronae selected because they were imaged by Magellan in stereo, that is very helpful in determining age sequences among the geologic units. We found in this study that we can describe the geology of coronae and their surroundings in terms of units we distinguished in our previous studies [3,4].

VERDANDI (5.5oN, 65.2oE, D = 180 km). Verdandi sits among the plains with wrinkle ridges (Pwr) embaying tessera (Tt) in the central part of Ovda regio. It is well seen in stereo that corona Verdandi is outlined by almost circular annulus standing over the surrounding Pwr plains. The corona floor is made of the same Pwr plains which is noticeably lower than the surrounding plains.Three quarters of the corona annulus are made of densely fractured terrain (COdf) with almost perfect concentric trend. Despite very close distance (5-20 km) between the corona annulus and tessera terrain no influence of the tessera structural pattern is seen in any corona element. COdf annulus is embayed from inside and outside by the Pwr plains. The wrinkle ridges that deform the Pwr plains trend mostly N-S and NE showing no alignment with the corona structure. In the SE part of the annulus there is a topographic gap filled by Pwr plains criss-crossed by the dense NE-trending fractures which are one of the branches of the Ix-Chel chasma rift zone. East of the corona several arcuate fractures concentric to corona and cutting the Pwr plains are seen. They are cut by another set of the rift-associated fractures.

THOURUS (6.5oS, 12.9oE, D = 290 km). Corona Thourus sits among plains with wrinkle ridges (Pwr). The corona annulus, which completely encircles the corona, is mostly made of densely fractured terrain (COdf) with almost perfect concentric structural pattern. It is well seen in stereo that the annulus stands over the surrounding plains and the corona interior is topographically lower than the surrounding plains.The COdf ring of the annulus is embayed by the materials of three sorts: 1) the material correlative to the fractured and ridged plains (Pfr) of [3,4], it participates in composing the annulus; 2) the material corelative to the shield plains (Psh) [4]; and the material of plains with wrinkle ridges (Pwr) which embays the corona annulus from outside and forms the dominant part of the corona interior. Pwr plains are deformed by wrinkle ridges with a predominantly E-W trend which slightly deflects to radial to the corona east and west of it. In the northern part of the corona interior there is 10x50 km area of relatively bright plains (not deformed by wrinkle ridges) correlative to the lobate plains (Pl) unit of [3,4]

BELET-ILI (6.0oN, 20.0oE, D = 300 km). This corona and neighboring corona Gaya (see below) are among the Pwr plains of the southern part of Berighinya Planitia. Belet -ili has an anulus consisting of different materials and structural features which form together the well visible quasi-circular structure: Pfr plains crossed by concentric fractures in the west, it embays a small massif of tessera terrain; Pwr plains deformed by concentric wrinkle ridges and concentric and radial fractures in the north; zigzaging wrinkle ridges in the east and concentric wrinkle ridges and inward-looking scarp in the south. The central part of Belet-ili corona is dominated by fields of numerous small shields correlative to the Psh plains. These fields are separated and embayed by the Pwr plains.

GAYA (3.5oN, 21.5oE, 350x500 km). Gaya corona is a pear shaped E-W elongated structure, sitting in the Pwr plains with subordinate Psh patches and outlined by sets of wrinkle ridges. The southern part of Gaya is outlined also by the well seen in stereo inward looking arcuate scarp. The the NW part of the Gaya annulus is simultaneously the southern part of the Belet-ili annulus. This connection looks as mutually concordant without any evidence of superposition. The SW part of the Gaya annulus is also encircled by a set of fine fractures concentric to general corona structure. The central part of corona Gaya are made of the Pwr plains with patches of densely (radially) fractured terrain (COdf) and fields of small shields (Psh) both embayed by Pwr.

ARAMAITI (26.3oS, 82.0oE, D = 350 km) and neigboring corona Ohogetsu (see below) are among the predominantly Pwr plains of Aino Planitia. In the vicinity and inside the corona there are two varieties of regional Pwr plains: the older having intermediate radar brightness (Pwr-i) and the younger which is noticeably darker (Pwr-d). The network of wrinkle ridges is superposed on both of them. Immediately east of Aramaiti there is a belt of fractured and ridged plains (Pfr) embayed by both varieties of the Pwr plains. It is well seen in stereo that at the north Aramaiti has two annulae divided by the trough and only one annulus at the south. The inner annulus of the corona north and the annulus of its south form together a spiral-like feature made of densely (concentrically) fractured terrain (COdf) which can be subdivided into two subunits: 1)COdf-a, which occupies the rimcrest of the first third of the mentioned COdf spiral, and 2) COdf-b which occupies the rest. COdf-a is more deformed, embayed by the Pwr-i plains and probably correlative to COdf/Pdf unit of [3,4]. COdf-b has a visible plain-like background with fine concentric lineaments and is the deformed Pwr-i plains. The SW sector of the inner annulus looks as arcuate plate of COdf-a upthrusted into SE direction (probably when the mentioned ridge belt was formed). Outer annulus of the northern part of Aramaiti is made of the Pwr-i plains cut by roughly concentric set of partly sinuous faults. The trough between the outer and inner annulae is filled with Pwr-d which embays both the faulted material of Pwr-i and the heavily deformed material of COdf-a. The corona core is a dome surrounded by the circular trough filled with Pwr-i and Pwr-d, as well as with younger radar dark flows (Pl-d). The domical core consists of Pwr-i, Psh and COdf-a materials. In the arcuate depression within the eastern segment of the annulus and outside the annulus are observed young dark plains of the type which was called by [5] as amoeboids (Pda) which are probably correlative to Pl/Ps

units [3,4].

OHOGETSU (27.0oS, 85.7oE, D = 175 km). It is the corona neighboring Aramaiti so regional geologic situation for Ohogetsu is mainly same as for Aramaiti. The most important difference is that corona Aramaiti sits aside of the belt with broad compressional ridges on it, while Ohogetsu is in between two segments of the belt. Corona Ohogetsu, like corona Aramaiti, has an annulus consisting of two varieties of the densely fractured terain: 1) COdf-a, 2) COdf-b. In SW sector of Ohogetsu there is a peculiar arcuate feature. On stereo it looks as a horse-shoe plate upthrusted upon the middle part of the SW section of the annulus. From consideration of local geology it was concluded that the plate material is probably the Pfr plains whose upthrust was due to the event of regional compression which formed the belt with broad ridges. Inner part of corona Ohogetsu is occupied by dark Pwr-d plains deformed by N-S trending set of wrinkle ridges extending southward into the area of Pwr-i plains. Among the Pwr-d plains of the corona interior there is a shield of about 10 km in diameter (Psh?). Western part of corona Ohogetsu annulus is flooded by the dark plains of the amoeboid type (Pda) which embays all the materials it is in contact including the Pwr-d plains and the wrinkle ridges themselves. To SE and SW of the corona annulus there are several localities of the lobate plains correlative to the Pl unit [3,4].

DISCUSSION AND CONCLUSION: The described observations on the age relations of different components of the studied coronae can be presented in a form of the following table:

Corona	Tt	COdf/Pdf	Pfr/RB	Pwr	Pl/Ps
Verdandi	n	//////////	?	n	n
Thourus	-	//////////	//////////	//////////	//////////
Belet-ili	n	?	//////////	//////////	n
Gaya	-	//////////	?	//////////	n
Aramaiti	-	//////////	?	//////////	//////////
Ohogetsu	-	//////////	//////////	//////////	//////////

Five of considered coronae consist of several material units and structures representing a time sequence of geologic events. Only Verdandi is an example of corona outlined by structures of one age deforming only one material unit. We found no evidence of coronae predating tessera and deformed by tessera terrain structure. The first evidence of a corona structure is a formation of an annulus due to warping of early regional and global units (Pdf; Pfr) of apparent volcanic origin. Following this initial stage, most corona annulae were flooded to different extents by regional volcanic plains (Pwr with patches of Psh). Then majority of the studied coronae experienced concentric and/or radial fracturing and with a half of them was associated the emplacement of flows otside and/or inside the corona. These later volcanics are unmodified by wrinkle ridges that relates them to rather recent period of geologic history of Venus. These observations are in agreement with our earlier results [2-4] and with results of other workers[1,6-9] so the general conclusion is that coronae are characterized by both local and regional structures and stratigraphic units and that their geologic history represents the interplay of local coronae events superposed on regional and global geologic evolution. Total life time of coronae in some cases (e.g. Vernandi) may span since early post-tessera period till pre-Pwr or even pre-Pfr time, that is probably less than 100 my, while in other cases (e.g. Ohogetsu) it is significantly longer, from early post-tessera time till post-Pwr, Ps/Pl time, that may be as long as 200 to 400 my.

REFERENCES: 1) Baer G. et al. JGR, 99, E4, 8355-8369, 1994; 2) Basilevsky A.T. Annales Geophysicae, Suppl. to vol. 12, C652, 1994; 3) Basilevsky A.T. & Head J.W. PSS, 43, N 12, 1523-1553, 1995; 4) Basilevsky et al. In: Venus II, The Univ. Ariz. Press, in press, 1997; 5) Head J.W. et al., JGR, 97, E8, 13153-13197, 1992; 6) Jackson E. et al., LPSC-26, 665-666, 1995; 7) Magee Roberts K. & Head J. GRL, 20, 1111-1114, 1993; 8) Magee K. & Head J. JGR, 100, 1529-1252, 1995; 9) Pronin A.A. Astron. Vestnik, 31, N1, 1997.

STEREO VIEW OF SIX CORONAE: A.T. Basilevsky and J.W. Head.

THE ANCIENT AGE OF MAXWELL MONTES, VENUS: PRESERVATION OF HIGH TOPOGRAPHY UNDER HIGH-SURFACE-TEMPERATURE CONDITIONS. J.D. Burt, J.W. Head, and E.M. Parmentier, Brown University (Dept. of Geological Sciences, Brown University, Providence, RI 02912 jburt@eos.hitc.com).

ABSTRACT: Maxwell Montes has the highest terrain and surface slopes of Venus, but displays little gravitational relaxation except on its northern and southern flanks [1]. Evidence that Maxwell is as old as the surrounding plains [2] leads to the challenge of explaining the preservation of high topography under conditions of surface temperature that would quickly cause the collapse of terrestrial mountain belts [3]. The dry diabase flow laws of Mackwell et al. [4] may provide the key to understanding this problem. Model results indicate that gravitational relaxation should not be important in changing the topography of Maxwell, if the mantle and crust of Venus are very dry.

BACKGROUND: Vorder Bruegge and Head [5] examine the implications of Airy support for Maxwell under conditions of low thermal gradients created by compressional deformation. At low strain rates thermal equilibration would permit volcanism to occur at the same time as mountain belt growth. Low viscosity of a deep crustal root would also promote gravitational collapse. At higher strain rates the thermal gradient would be depressed, preserving the strength of crustal root and delaying igneous activity. Therefore, they favor rapid construction of Maxwell because the mountain belt lacks evidence of simultaneous deformation and volcanism. Additionally, at low temperatures the gabbro-eclogite phase change occurs slowly, but the transformation of deep crustal material would eventually reduce topography.

Namiki and Solomon [6] investigate further the role of the gabbro-eclogite phase change in determining the mountain belt topography. The possible low water abundance on Venus may mean the gabbro-eclogite phase change occurs there by solid state (volume) diffusion rather than grain boundary diffusion, inhibiting the rate of the transition and preserving metastably basaltic crustal material within the stability zone of eclogite in mountain roots. They conclude that rapid mountain belt formation, resulting in low thermal gradients, favors metastable gabbro in the crustal root and preserves high topography, implying that Maxwell must be young relative to the surrounding plains. The lower elevations of volcanically active Danu may illustrate the effects of the temperature-enhanced phase change limiting elevations. Also, a young Maxwell would be consistent with the undeformed appearance of Cleopatra crater.

In contrast, Basilevsky [2] finds stratigraphic evidence that Maxwell is at least as old as neighboring ridged plains. He interprets this as evidence that Maxwell is as old as the estimated surface age of 0.3 to 0.5 Ga [7, 8] and that low water abundance allows high topography and steep slopes to last for geologically long periods. Meanwhile, Herzog et al.[9] point out that the high surface atmospheric pressure would prevent exsolution of H_2O for abundances below about one weight percent. The dry atmosphere could thus be consistent with hydrous minerals existing in the venusian mantle. This represents a volatile source capable of expediting the gabbro-eclogite phase change. If so, high topography may be dynamic, limited by the balance between rate of elevation increase and the rate of eclogite formation.

Smrekar and Solomon [1] have investigated the evidence for gravitational relaxation in Maxwell. While extensional features can be found on the northern and southern flanks of the belt, the western slopes, where the steepest slopes occur, bear no recognizable evidence of relaxation. They model viscous relaxation of topography, invoking the flow law of Caristan [10] for Maryland diabase. They predict that gravitational spreading is likely to occur on a time scale shorter than the mean surface age indicated by the crater statistics. They conclude that dynamic tectonic support may be necessary to preserve the high topography and slopes of the mountain belts.

Freed and Melosh [11] modelled the gravitational collapse of Ishtar Terra. Building on the work of Smrekar and Solomon [1], they find that the dry flow law of Mackwell [4] permits the crust to be sufficiently viscous to support Ishtar's topography for periods on the order of 500 million years.

We have formulated two simple models to explore the role of the dry mantle viscosities in the support of Maxwell. Assuming Maxwell topography is supported by thickness variations in a basaltic crust we calculate the stress distribution for periodic topography having a wavelength similar to that of Maxwell. A steady-state thermal gradient should apply if Maxwell is old. This allows for estimation of the crustal viscosities beneath the belt and estimation of the rate of collapse of the topography.

THEORETICAL MODEL: A simple assessment of the age of Maxwell can be obtained using a model for viscous flow in response to a surface load [12]. Assuming a periodic surface load of the form

$$\omega = \omega_0 \rho g \cos\frac{2\pi x}{\lambda}$$

where ω_0 is the amplitude of the surface load or topography, and λ is the wavelength, the characteristic relaxation time is given by

$$\tau = \frac{4\mu\pi}{\rho g \lambda} .$$

If the wavelength of Maxwell is assumed to be $\lambda = 1000$ km, $\rho = 3$ gm/cm^2 and μ to be 10^{21} Pa s, the relaxation time is 1.2×10^4 years. For Maxwell to have a relaxation time on the order of 10^9 years the viscosity would be 8×10^{25} Pa s.

Mackwell et al. [4] provide flow laws appropriate to materials subject to the dry conditions of Venus. Their flow law for Maryland Diabase is

$$\varepsilon = 4.2\, \sigma^{5.1} \exp -\left(\frac{505}{RT}\right),$$

where ε is the strain rate, σ the differential stress in MPa, R the gas constant, and T the temperature. This can be rewritten, for this model, and using the second invariant of the stress tensor, as

$$\varepsilon = 4.2\left[\rho g \ \omega_o \ y \ \frac{2\pi}{\lambda} \ \exp - \left(\frac{2\pi y}{\lambda} \right) \sqrt{2} \right] \qquad 4.2$$

$$\left(\rho g \ \omega_o \ y \ \frac{2\pi}{\lambda} \cos \frac{2\pi x}{\lambda} \ \exp - \left(\frac{2\pi y}{\lambda} \right) \right) \exp - \left(\frac{505}{RT} \right)$$

From this relation μ can be derived

Using viscosities for a thermal gradient governed by basaltic crustal radioactivity, a surface temperature of 750 K, and a uniform mantle temperature of 1321 K below 200 km depth, the relaxation rate for Maxwell can be evaluated. A mid-crustal viscosity can provide an estimate of the relaxation time. Assuming Maxwell to be in isostatic equilibrium a maximum crustal thickness is about 120 km. The viscosity for the 60 km depth is $\mu = 10^{25.6}$Pa s, yielding a characteristic relaxation time of about 5 x 10^8 years. This is close to the value that is required to maintain the topography of Maxwell for 10^9 years.

If gravitational collapse may happen slowly enough to permit Maxwell to retain its high elevations, the transformation of gabbro to eclogite may become more important. A characteristic reaction time for the conversion from one phase to the other can take the form

$$\tau = \frac{\delta^2}{D}$$

where τ is the characteristic reaction time, δ is the grain size, and D is the diffusion coefficient. Taking $D_{Al,\ Opx}$ as given in Namiki and Solomon [6] as a lower bound,

$$D_{Al,\ Opx} = 1.1 \times 10^{-5} \exp\left(\frac{-400\ kJ}{RT} \right)$$

an estimate can be made of the reaction time for a given temperature. At the base of the crust the temperature is about 925 K. At this temperature, the reaction time is on the order of 10^{14} years. Clearly this indicates that the phase change happens too slowly to significantly affect the isostasy over periods as short as a billion years.

This simple modeling is based on a formulation assuming uniform, not variable, viscosity. To more accurately determine rates of relaxation for a model in which the viscosity varies with temperature, numerical models are necessary.

NUMERICAL MODEL: In a model region measuring 1000 km wide and 1000 km deep, and having an imposed surface load of the form

$$\omega_o \rho g \cos \frac{2\pi x}{\lambda} ,$$

we solve for fluid flow using a Lagrangian finite element method. A free surface and free-slip vertical and basal boundaries comprise the boundary conditions. The imposed depth-dependent viscosity is derived from the flow law of Mackwell et al. [4]. Flow calculations result in estimates of the surface vertical velocity component.

To evaluate the rate of collapse we again appeal to the simple theory. Since the rate of change of the vertical displacement (the vertical velocity) is given by

$$\frac{\delta\omega}{\delta t} = \frac{\rho g \lambda}{4\pi\mu} \ \omega_o \ \exp - \left(\frac{\rho g \lambda}{4\pi\mu} \right) ,$$

then

$$v = -\frac{1}{\tau} \omega_o \exp\left(\frac{-t}{\tau} \right) .$$

At t = 0 this simplifies to

$$v = -\frac{\omega_o}{\tau} .$$

The model calculates the amplitude of the v component of the surface velocity to be 1.2 x 10^{-1} This produces a characteristic relaxation time of 10^{11} years.

CONCLUSIONS: While these models are complicated, they do provide an estimation of the r collapse of Maxwell Montes. These results indicat gravitational relaxation should not be importa changing the topography of Maxwell, if the mantl crust of Venus are very dry. If significant water do exist within the interior of Venus, then the mantl crust are strong and the rate of the gabbro-eclogite change is very low. Both of these factors would cont to the preservation of high topography despite the temperatures of the venusian surface. If hydrous mi exist [9] within the mantle, however, dy mechanisms may be required to explain the existen old high topography.

REFERENCES

[1] Smrekar, S.E. and S.C. Solomon, (1992) JGR 16121; [2] Basilevsky, A.T., (1995) LPSC 26: Weertman, 1979; [4] Mackwell, S.J. et al., (1994) 25: 817; [5] Vorder Bruegge, R.W., and J.W. Hea (1991) Geology 19: 885; [6] Namiki, N., and Solomon, (1993) JGR 98, E8: 15025; [7] Schaber, G. al., (1992) JGR 97, E8: 13257; [8] Strom, R.G. e (1994) JGR, 99, E5: 10899; [9] Herzog, S.G. e (1995) LPSC 26: 591; [10] Caristan, Y., (1982) JGI 6781 ; [11] Freed, A.M., and H.J. Melosh, (1995) 26: 421; [12] Turcotte, D.L. and G. Schubert, (1 Geodynamics Applications of Continuum Physic Geological Problems, John Wiley & Sons, New 1982;

Timescale of Regional Plains Emplacement on Venus Geoffrey C. Collins[1], James W. Head[1], Mikhail A. Ivanov[2], and Alexander T. Basilevsky[2]. [1]Brown University, Dept. of Geological Sciences, Providence, RI 02912, [2]Vernadsky Institute, Russian Academy of Sciences, Moscow, Russia; Geoffrey_Collins@brown.edu.

An outstanding question in the Venus resurfacing debate is the length of time over which a theoretical "catastrophic" resurfacing event may have occurred. The emplacement of the wrinkle ridged plains over ~70% of the planet occurred synchronously over large areas [1,2] and was an important part of the global event. The length of time over which the wrinkle ridged plains were emplaced can be constrained by the number of creaters which they embay. Most of the embayed craters on Venus are embayed by lobate plains from local volcanic sources, and only 5-8 craters are embayed by the vast regions of wrinkle ridged plains [3]. The model of Strom et al. [4] estimates the length of the resurfacing episode based on how many craters it embayed, but this model was based on resurfacing by small, randomly distributed volcanic flows. This does not agree with observations of the nature of the wrinkle ridged plains, which the plains appear to be simultaneously emplaced over extensive areas [2]. Here we develop a simple statistical model based on the plains flooding of extensive areas in order to constrain the length of time over which they were emplaced.

One end-member model would be to assume that these 5-8 craters embayed by wrinkle ridged plains represent the entire population of craters on the surface below the plains. This implies that all of the wrinkle ridged plains are thin enough that they did not completely bury the smallest craters. On the other extreme, the plains could have buried all preexisting craters, and the embayed craters we see were formed on the plains during their emplacement. The relative roles of these two end-member models can be examined by estimating the depth of wrinkle ridge plains deposits by a means independent of craters. We have mapped an area extending from 23°-35° N latitude, covering over 8% of the planet. This area is composed of 37.7% material older than plains with wrinkle ridges, 10.3% material younger than the plains, and the other 52% is plains with wrinkle ridges. The plains with wrinkle ridges were separated into areas thinner and thicker than 500 meters. This depth contour was obtained by assuming that the topography of the older material underlying the plains sloped away from every surface contact with the wrinkle ridged plains at a 1% grade (0.57° angle). This will probably give an overestimate of the depth of the wrinkle ridged plains, since only 14% of the Venusian surface has regional slopes above 0.24° [5], and the only features on Venus with slopes consistently above this 0.57° value are the mountains around Ishtar Terra [6]. Using this slope assumption, 63% of plains with wrinkle ridges in this mapping area are thinner than 500 meters, and 37% are thicker than 500 meters. The depth of 500 meters was used as a cutoff value because the rims of median-size (30 km diameter) or larger craters are about 500 meters high, as deduced from topographic profiles of craters generated by Sharpton [7]. Plains thinner than 500 meters should be thin enough for the rims of median-size craters or larger to show through, so at least half of the preexisting population of craters below the plains will show through as embayed craters in these shallow areas. We will assume that plains thicker than 500 meters will have buried all underlying craters. All of these assumptions: the steep underlying slopes, the burial of all craters in thick plains, and the burial of all small craters in thin plains, will tend to overestimate the number of craters destroyed by the emplacement of wrinkle ridged plains, thus making the resulting timespan a maximum estimate. The eight craters possibly embayed by wrinkle ridged plains occur in areas mapped in this scheme as thin plains. Five of the eight craters are larger than median diameter.

If 70% of the surface of Venus is covered by wrinkle ridged plains and 63% of these plains are thinner than 500 meters, 44% of the surface is covered by wrinkle ridged plains thinner than 500 meters. The probability is .44 that a crater emplaced randomly on the surface falls within this area. Since only craters larger than median size are guaranteed to be unburied within this area, the probability is .22 that a crater emplaced on the surface

during the timespan in question will be embayed but not buried by wrinkle ridged plains. Since we observe five craters of median diameter or larger embayed by thin areas of wrinkle ridged plains, we can calculate the probability that, given a number of craters emplaced on the surface, exactly five will be larger than median diameter, in the area of thin plains. This gives an expected value of 22 craters, with a 98% confidance interval of 10-54 craters. In terms of a percentage of the mean age of the surface of Venus (300-500 Ma), the expected value is 2.4% (7-12 Ma), with a lower limit of 1% (3-5 Ma) and an upper limit of 5.8% (17-29 Ma). This timespan represents the age of the surface upon which the wrinkle ridged plains were emplaced plus the length of the emplacement of wrinkle ridged plains.

Most of the wrinkle ridged plains are thin enough that a large number of underlying craters would not have been completely buried, but only embayed by their emplacement. Since so few craters are observed to be embayed by these thin plains, they must have formed over a short time on a young surface, covering a 5-30 Ma timespan. The emplacement of these plains was not the prime mechanism for removing the ancient population of craters. An event must have occurred prior to the emplacement of these plains to erase the ancient population. Resurfacing such as tectonic resurfacing, which may have erased the ancient crater population from the tessera [8] or volcanic resurfacing by stratigraphically lower plains units, must be the primary mechanisms responsible for the young surface age observed on the surface of Venus. The wrinkle ridged plains which cover the majority of the surface of Venus are only a relatively thin veneer which formed quickly and did little to rejuvenate the surface.

References: [1] Basilevsky, A. T., and J. W. Head (1995), *Planet. Space Sci.* 43, 1523-1553; [2] Basilevsky, A. T., and J. W. Head (1996), *Geophys. Res. Lett.* 23, 1497-1500;.[3] Collins, G. C., et al. (1996), *LPSC XXVII*; [4] Strom, R. G., et al. (1995), *J. Geophys. Res.*, 100, 23,361-23,365; [5] Sharpton, V. L., and J. W. Head (1985), *J. Geophys. Res.* 90, 3733-3740; [6] Sharpton, V. L., and J. W. Head (1986), *J. Geophys. Res.* 91, 7545-7554; [7] Sharpton, V. L. (1994), *in* Dressler, B. O., et al., eds., *Large Meteorite Impacts and Planetary Evolution*, GSA Special Paper 293; [8] Solomon, S. C. (1993), *LPSC XXIV* 1331-1332.

REMOTE AND LOCAL STRESSES AND CALDERAS ON MARS;

L. S. Crumpler[1], J. C. Aubele[1], and J. W. Head[2]; (1)New Mexico Museum of Natural History and Science, 1801 Mountain Rd NW, Albuquerque, NM 87104; (2)Dept. of Geol. Sciences, Brown University, Providence, RI 02912; crumpler@nmmnh.-abq.mus.nm.us

INTRODUCTION. The detailed structure of calderas is a sensitive indicator of the stress environment existing at the time of caldera formation. Unlike regional patterns of strain, such as wrinkle ridges, graben, and fractures, calderas, however, have short time scales for formation and record local stress at essentially point sources. Strain associated with caldera formation and evolution may also be tied stratigraphically to a relatively well-defined geologic unit and well-constrained times. In the following, we have compiled the structural characteristics of calderas on Mars [1] and compared the deduced orientation of remote stress with predicted patterns of global strain, patterns attributable to regional slopes, and patterns attributable to relict or pre-existing substrate structure.

OBSERVATIONS. Several types of structure alignment can be distinguished in the summit calderas of the larger martian volcanoes: (1) overlapping calderas, (2) concentrations of pits and channels on flank sectors, and (3) linear, through-trending fissure patterns. Overlapping and elongated calderas characterize the summits of Olympus Mons and the Tharsis Montes (Figure 1). These patterns are most prominent in larger edifices or the larger calderas that are indicative of large magma reservoirs. Calderas associated with smaller volcanoes, such as Biblis Patera, Ulysses Patera, Ceraunius Tholus, and Albor Tholus are either circular or consist of randomly overlapping caldera segments.

ANALYSIS. Caldera structures preserve regional stress patterns because dikes develop along directions of maximum principal stress. Systematic alignments therefore tend to develop in successive magma reservoirs within an evolving magmatic system [2]. The principles of dike emplacement were reviewed previously [3] and are here briefly re-iterated. A dike is propagated from a magma body, resulting in magma being either erupted at the surface or injected laterally, when the wall failure criteria $P_l + P_m \geq |s_3| + T$ is satisfied [4] and magmatic pressure exceeds the sum of remote stress (minimum compressive stress, s_3) and tensile strength (T) of the country rock. Regional patterns of stress that may influence the orientation of s_3 can arise from strains resulting from either tectonic processes, local and regional relief, or pre-existing, directional variations in the value of T (i.e., pre-existing structural fabrics)[5]. All of these are predicted to have a significant influence on regional stress arrangements on Mars [6,7,8]. The influence of regional topography and its associated stress patterns on dike orientation has been used previously in assessing the orientations of possible dike-related graben sets on Venus [9]. On Mars, basins and basin structures are also likely to be important.

Figure 1 is a comparison of predicted patterns of minimum stress from global topographic relief [8] with orientations of the minimum stress determined from the relevant s_3 indicators (overlapping calderas, concentrations of pits and channels on flank sectors, and linear, through-trending fissure patterns).

DISCUSSION. Calderas are limited in absolute number , so the results of a comparison between observed and predicted patterns are of limited quantitative value. However, logical geologic inferences of regional interest can be made based on observed structure and local/regional associations. The salient points are reviewed in Table 1 which summarizes the principal inferences.

Table 1. Three caldera strain/remote stress associations:

Volcanoes	Timing	Origin of Stress
[AM, PM, AM, Uranius Patera, Hecates, Elysium]	mid-age volcanoes	regional dynamic lithospheric flexural stress
OM, Tharsis Tholus, Ceraunius Tholus	mid and young age	local crustal gravity stress (regional slope and edifice effect)
Tyrrhena, Nili, Meroe, Hadriaca, Peneus, Amphitrites]	old to mid age	regional inheritance from pre-existing structure
[Biblis, Albor, Jovus, Apollonaris, Alba(?)]	old	No (or little) apparent local or regional

Patterns of strain associated with the larger calderas follow stresses predicted from global isostatic flexure patterns [6,7,8] particularly within the large volcanic rises of Tharsis. Notable exceptions in Tharsis include Olympus Mons, Tharsis Tholus, Alba Patera, and Ceraunius Tholus. Fractures obeying the predicted pattern of strain occur around Alba Patera, but do not appear to have operated at the time of magma emplacement. At Olympus Mons, large gravity stresses associated with regional slip of the edifice on the slopes of Tharsis may have dominated the local stress field [9]. This also appears to be the case for Tharsis Tholus.

Patterns of deformation in older calderas may relate to regional and local slope effects. The oldest, and lowest, calderas appear to have been influenced by pre-existing structural fabrics associated with basins.

REFERENCES CITED. [1] Crumpler, et al, 1995, *Lunar Planet. Sci.*, XXVI, 305-306; Crumpler et al., 1994, *Lunar Planet. Sci.* XXV, 305-306; Crumpler, et al, 1995, *Geol. Soc. London Spec. Pub. 110*, 307-347; Crumpler, et al., 1990, *MEVTV Workshop on the Evolution of Magma Bodies on Mars*, Richland, 14-15; [2] Pollard, and Muller, 1976, *Jour. Geophys. Res.* 81, 975-984; Nakamura, 1982, *Bull. Volc.Soc. Japan*, 25, 255-267; [3] Crumpler, Head, and Aubele, 1996, *LPSCXXVII*, 277-278; [4] Gudmundsson, 1988, *J. Volc. Geoth.Res*, 35, 179-194; [5] Nakamura, 1977, *J. Volc. Geotherm. Res.*, 2, 1-16; [6] Banerdt et al., 1982, *Jour. Geophys. Res.*, 87, 9723-97-33; [7] Phillips and Lambeck, 1980, *Rev. Geophys. Sp. Phys.* 18, 27-76; [8] Sleep and Phillips, 1985, *Jour. Geophys. Res.*90,4469-4489; [9] McGovern and Solomon, 1993, *Jour. Geophys. Res.* 98, 23553-23579.

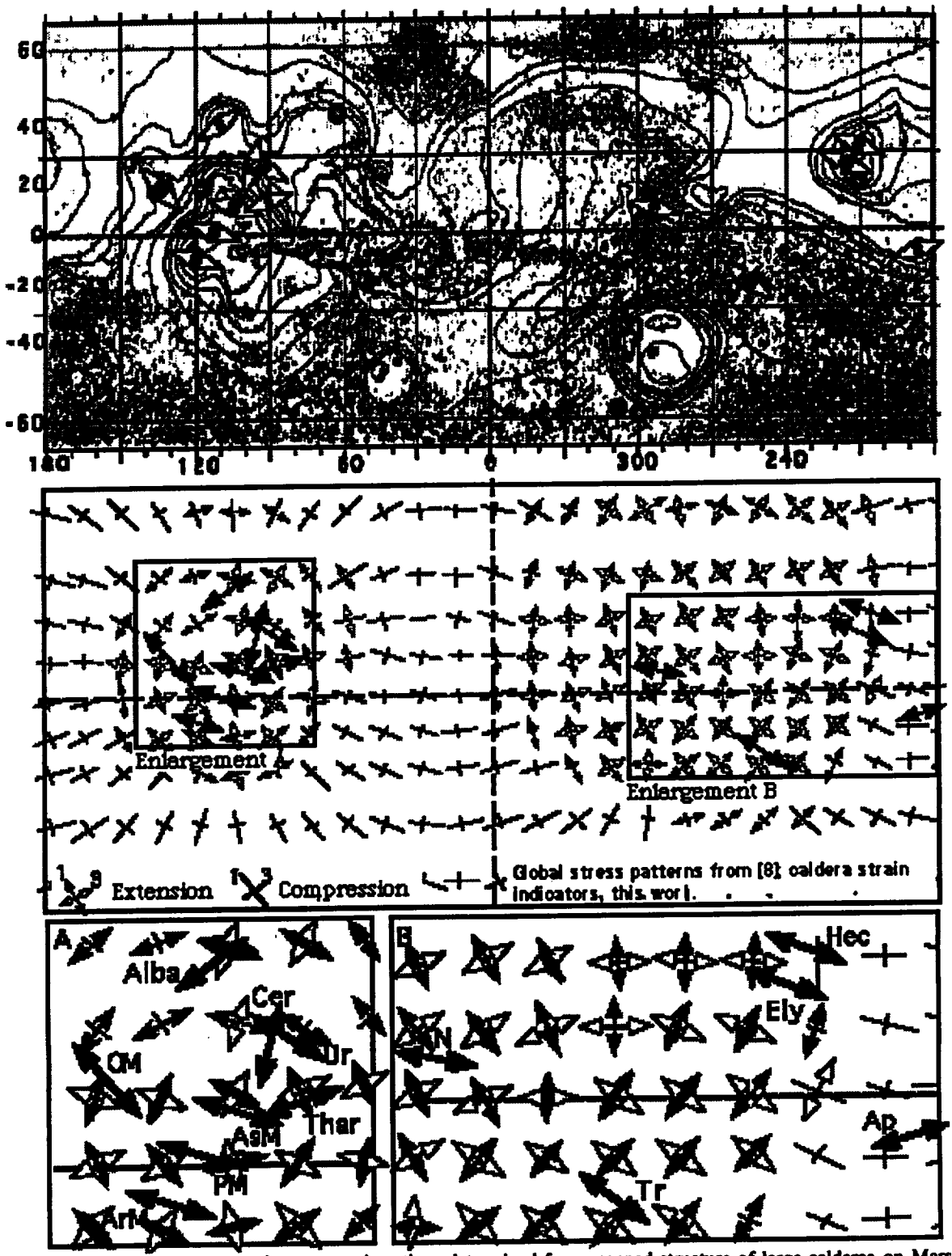

Figure 1. Top: Minimum compressive stress orientations determined from mapped structure of large calderas on Mars [1 Center: Stress orientations superimposed on global stress field predicted from topography [8]; bottom: Enlargement c main volcanic regions. Observed orientations are consistent with remote stresses predicted from isostatic flexure in man cases, but some calderas appear to have been strongly influenced by stresses within the crust due to slope and azimuth: variations in crustal strength.

LUNAR LINEAR RILLES, MODELS OF DIKE EMPLACEMENT AND ASSOCIATED MAGNETIZATION FEATURES. J. W. Head[1], L. Wilson[1,2] K. A. Anderson and R. P. Lin[3]; [1]Department of Geological Sciences, Brown University, Providence, RI 02912 USA; [2]Environmental Science Division, Institute of Environmental and Biological Sciences, Lancaster University, Lancaster LA1 4YQ, UK; [3]Space Sciences Laboratory, University of California - Berkeley, Berkeley, CA 94720.

Introduction and Background: Lunar linear and arcuate rilles form from tectonic deformation associated with near-surface stress fields [1, 2] which have been attributed a variety of origins, including lithospheric flexure in response to mare basalt loads [3], and to the emplacement of dikes to near-surface environments [4]. We have been assessing the nature of dike intrusion as a source of near-surface stress fields sufficient to produce linear rilles [4, 5] and conversely, developing criteria to distinguish rilles plausibly cause by near surface dike intrusion from those formed by other mechanisms [6]. We have developed model predictions [5], photogeologic criteria [6], and have most recently been investigating the possibility of using measurements of magnetic fields by the electron reflection method to aid in the identification of candidate linear rilles formed by dike intrusions [4]. In this abstract we report on progress in the further assessment of data from these sources and on the identification of areas in which magnetization features appear to be associated with linear rilles.

Theory, Predictions, and Observations: A dike propagating from depth toward the surface generates a stress field in the surrounding rocks. As an upward-propagating dike nears the free surface, the accompanying stress field is progressively modified; stresses and associated strains at the surface become concentrated in two regions parallel with the strike of the dike plane and located on either side of the line of the potential outcrop of the dike on the surface. The separation on the surface between the zones of maximum elastic stress is essentially independent of the mean dike thickness and depends only on the dike tip depth [7]. However, the magnitude of the maximum stress is directly proportional to the dike thickness, as well as being dependent on the depth of the dike tip. As a dike tip rises towards the surface the stresses become sufficiently large that failure of the country rocks takes place in shear or tension at points well outside the process zone on both sides of the dike. Whether these initial failures are actually on the surface or at some finite depth below it is a function of relationships between the excess pressure within the dike, the dike width and the mechanical properties of the country rocks [8]. The failure planes soon intersect the surface, however, and a linear graben structure begins to develop. If the dike stalls at a sufficiently great depth there will be some undetectable small amount of surface extension and uplift. Shallower penetration will lead to a volume of melt being exposed to the relatively low pressure environment near the surface and will encourage the generation of a greater mass of CO since the chemical reaction producing it is pressure-dependent [9]. Sufficiently close approach of the dike tip to the surface will cause new fractures to form and allow significant movements along parallel faults to occur. As the dike tip further approaches the surface, the main effect will be for the graben to become progressively deeper as more strain is accommodated. Very shallow intrusion may lead to further fractures developing on the floor of the graben and will encourage the formation of small secondary intrusions and possible eruptions.

These theoretical predictions support the idea that linear rilles may be the sites of subsurface dike emplacement. Specifically, from a morphological point of view, many dikes may intrude to sufficiently shallow depths that they will create graben, but there will be no surface evidence of eruptions. These are clearly the most difficult to distinguish from graben formed from stress fields not related to dikes. Several examples are known in which other evidence suggests that dikes exist below the observed graben. Rima Sirsalis, a 380 km long graben in the highlands, is characterized by a linear magnetic anomaly interpreted to be due to an underlying magnetized dike [10, 11, 4]. Thus, magnetometer and electron reflection experiments may provide additional information on the location of buried dikes and the origin of specific graben. A reasonable interpretation of this relationship is that the impact event excavated mare material from the top of a dike underlying the graben. In some cases, dikes may propagate sufficiently near to the surface to create a graben, but still not cause significant eruption of lavas [12]; in these situations, degassing of the upper part of the dike may cause the formation of gas/magma mixtures which might buoyantly rise to the surface or be forced to the surface through overpressurization of the upper part of the dike. In this particular configuration, the distribution of stresses anticipated in the vicinity of the dike tip can cause migration of magma and exsolved gas from the upper part of the dike to locations outward of the main graben bounding faults, a phenomenon likely to explain the distribution of cones at Rima Parry V [4]. Dikes reaching closer to the surface, but still not having associated extensive lava flows, should produce narrower graben, and any pyroclastic cones should be more closely associated with the graben.

Observations and Analysis: On the basis of the likelihood that numerous linear rilles could represent the surface manifestation of dikes emplaced to the vicinity of the lunar surface, and the fact that in at least one place on the Moon where there is a good correlation between a linear magnetization anomaly and a linear rille [10, 11], we have been reanalyzing data from Apollo magnetometer and electron reflection experiments to assess whether they can provide additional information on the location of buried dikes and the origin of specific graben. The method of

measuring lunar magnetic fields by the electron reflection method has been described elsewhere [10, 13, 14].

Rima Sirsalis is the site of a strong local magnetic field [10, 11] (Figure 1). It is a NE trending linear rille about 380 km in length located in the highlands south of Grimaldi (Figure 1); it averages less than 4 km wide and is 150-250 m deep. The depth to the dike top is estimated to be ~1700 m and dike width is estimated to be in the range 600-700 m [4]. These values compare with predicted dike widths of 600-800 m for dikes propagating from parent magma bodies at depths up to 300 km [15]. The magnetic data for Rima Sirsalis can also be used to estimate the average width of the subsurface dike given suitable assumptions about its magnetic properties. Srnka *et al.* [11] used various configurations of single and multiple dikes extending to various vertical depths from the surface and having various degrees of magnetization. Using a single dike model exemplified by their Figure 7 and varying the mean dike width and a range of remanent magnetization values it was found [4] that a mean dike width of ~430 m is consistent with the measurements if the magnetization. Thus, on the basis of these considerations, we conclude that a dike emplacement model for the Sirsalis graben and magnetic anomaly is plausible.

An additional anomaly is observed over the Fra Mauro/Bonpland region (Figure 1) where the reflection coefficient is distinctly above background but less than a factor of two of that seen at Rima Sirsalis. A large concentration of linear rilles is seen in this area. Rima Parry V, about 50 km in length, is a linear rille that is part of a series of graben-like features that cut the floors and rims of the craters Fra Mauro, Parry, and Bonpland. It begins in the south on the floor of Bonpland in the vicinity of Rima Parry VI, and extends NNE across the northern rim of Bonpland, descending to the floor of Fra Mauro, and continuing across the floor until it merges tangentially with the NNW trending Rima Parry I. Midway between the ends of the rille, the rille walls are obscured by deposits associated with a set of volcanic cones parallel to the western rille margin. Rilles in the vicinity of Rima Parry V cut the early Imbrian Fra Mauro Formation and are embayed by later Imbrian-aged maria [16]. On the basis of observations and empirical relationships, the average dike width is estimated to be about 150 m [4]. The estimated depth to the dike top is ~750 m. Thus, on the basis of these considerations and the presence of associated pyroclastic deposits, we conclude that the characteristics of Rima Parry V, and by association the adjacent rilles, are consistent with formation by dikes which propagated from depth to near the lunar surface. The lower reflection coefficient values than at Sirsalis may be related to the smaller dike widths.

Preliminary Conclusions: On the basis of this analysis, we find that one of the prime candidates for linear rilles associated with dike emplacement on the basis of morphology and geology (e.g. Rima Parry V and associated rilles) is also characterized by a magnetic field anomaly plausibly attributed to magnetization of the dike. We are presently examining the area in more detail to correlate individual peaks with local features, and extending the analysis to other areas of the lunar surface covered by the Apollo 15 and 16 data.

References: 1] Golombek, M.P., *JGR, 84*, 4657, 1979; 2] McGill, G. E., *Icarus, 14*, 53, 1971; 3] Solomon, S.C. and Head, J.W., *RGSP, 18*, 107, 1980; 4] Head, J. and Wilson, L., *PSS, 41*, 719, 1993; 5] Wilson, L. and Head, J. W., *LPSC 27*, 1445, 1995; 6] Head, J. and Wilson, L., *LPSC 27*, 519, 1996; 7] Mastin, L. and Pollard, D., *JGR, 93*, 13221, 1988; 8] Melosh, H. and Williams, D. *JGR, 94*, 13961, 1989; 9] Sato, M., *Eos, 58*, 425, 1977; 10] Anderson, K. et al., *EPSL, 34*, 141, 1977; 11] L. Srnka et al., *PEPI, 20*, 281, 1979; 12] J. Mustard and J. Head, *LPSC 26*, 1023, 1995; 13] Howe, H. et al., *GRL, 101*, 1974; 14] Anderson, K. et al., *Space Sci. Instr., 1*, 439, 1976; 15] Head, J.W. and Wilson, L., *G&CA, 56*, 2155, 1992; 16] Wilhelms, D. E., The geologic history of the Moon, *U.S.G.S. Prof. Paper 1348*, 302 p., 1987.

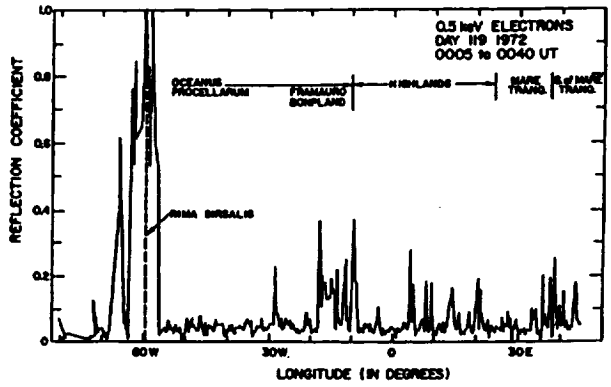

Figure 1.

STRATIGRAPHICAL CONSTRAINS ON THE DURATION OF TESSERA FORMATION: PRELIMINARY RESULTS OF THE REGIONAL MAPPING OF VENUS

M.A.Ivanov[1] and J.W.Head[2]. [1]Vernadsky Institute, Russia Academy of Sci., 117975; [2]Dept. of Geol. Sci, Brown Univ., Providence, RI 02912

Introduction

Tessera is a geologic unit, the surface of which is heavily deformed by tectonics [1-4]. By definition, two sets of tectonic features must be on the tessera surface. Besides tessera, there are other tectonically deformed terrains on Venus. However, they possess simpler structural patterns compared with tessera. The geological mapping of many areas on Venus has shown that the tessera with its characteristic tectonic pattern (normal tessera) always makes up the base of the local and regional stratigraphic columns [5-11] even though there are several different styles of tectonic activity [4,12]. Such a stratigraphic position gives the possibility to date the tectonic episode of tessera formation as occurring at the beginning of the visible geologic history of Venus [10,11].

We have conducted detailed geologic mapping within a zone from 0 to 360E, 22.3 - 37.6N. The mapping showed that there are terrain types the tectonic pattern of which satisfies the formal definition of tessera but is simpler and morphologically close to the pattern of younger and less deformed units. This terrain, quasitessera or tessera-like terrain, may both represent facies of the normal tessera and illustrate stages of tessera formation. Analysis of quasitessera morphology, geologic position, and areal distribution could help to answer the question: How did the intensity of tessera formation change through the visible part of Venus' geologic history?

Global stratigraphic scheme of Venus

To answer the above question it is necessary to understand the stratigraphic position and morphologic nature of quasitessera. The stratigraphic column consists of the units which are as follow (from older to younger) [10,11,13,14]. Tessera terrain (Tt). Densely fractured plains (Pdf) are the plains deformed by dense and narrow parallel fractures. Pdf embays tessera and is embayed by younger plains. Fractured and ridged plains (Pfr) / Ridge Belts (RB) presented by plains occasionally deformed by broad ridges. RB are tectonic facies of Pfr characterizing by densely packed broad ridges. Pfr/RB embayed by younger plains and embays Tt and Pdf. Fracture Belts (FB). This unit had formed by disruption of the older material units. The unit presented by swarms of fractures and graben. Shield plains (Psh) presented by plains with numerous shield-like features. Psh embays Pdf, Pfr, and the majority of the FB and is embayed by younger plains. Plains with wrinkle ridges, lower and upper members (Pwr1-2) are morphologically smooth plains moderately deformed by wrinkle ridges. Plains with wrinkle ridges embay the all above units. Lobate plains and Smooth plains (Pl/Ps) have morphologically smooth surface mostly undisturbed by tectonic features. Pl/Ps embays wrinkle ridges of Pwr.

Description of the tessera/ non-tessera transitions C1-30n009

There are fragments of elevated terrain with rough surface typical of tessera. However, the terrain has only one set of deformation (fractures) which is characteristic of Pdf. C1-30n027: There are Tt, Pdf, and Pfr and there is no quasitessera here. C1-30n045: Tt, Pdf, and Pfr are presented here. One fragment of Pdf is cut across by a graben. The graben complicates the fragment's surface and makes it to be looking like tessera. There is no transition between tessera and Pfr/RB. C1-30n063: There are occurrences of Tt, Pdf, and Pfr. In several places contacts between Tt and Pfr are gradual. Some occurrences of Pfr look like tessera due to their brightness and complex deformational pattern but there is no gradual transitions between Tt and Pdf. C1-30n081: Tt presented by the southern portion of Tellus, boundary of which is heavily embayed by the variety of units. Pfr embays the tessera. At the contact both Tt and Pfr are cut by fractures which make the Pfr pieces to be looking like tessera. C1-30n099: Some fragments of Pfr at the tessera boundary have two sets of structures (ridges and fractures) and resemble tessera but have lower density of tectonical structures and more regular pattern of deformation. Pdf has no the transitional facies with Tt. C1-30n117: Pfr is occasionally in contact with Tt. Sometimes the ridges typical of Pfr disrupted orthogonally by graben. This makes the occurrences of Pfr to be look like tessera. Although Pdf also occurs, the unit has no facies transitional to tessera. C1-30n135: Pdf is sometimes in contact with Tt. At the contact the chaotically deformed tessera merge gradually with Pdf which further from the contact possesses only one set of deformation. Pfr is spatially associates with tessera but has no transition facies with Tt. C1-30n153: There is no tessera in this C1. Fragments of radar bright terrain with two sets of extensional features and remnants of lava plains are visible. The terrain fits the formal definition of tessera but demonstrates more regular pattern of deformation. C1-30n171: There are Tt, Pdf, and Pfr. Small fragments inside tessera with two sets of extensional structures resemble the deformational pattern of both tessera and Pdf. There is no transition between tessera and Pfr. C1-30n189: Within the occurrences of Pfr there are areas resembling tessera by two sets of compressional and extensional features. In the contrast to tessera, the areas have diffuse boundaries. There is no transition between Tt and Pdf. C1-30n207: Pdf and Pfr have no transitions with Tt. C1-30n225: There is a little of tessera and no the transitional facies between Tt and other units. C1-30n243: There is the gradual transition between Pdf and Tt along the contacts between the units. C1-30n261: There are a few isolated fragments of terrain which shares common characteristics of Tt and Pdf: It is radar bright, elevated, deformed by several sets of fractures, and generally has the morphology typical of the lava plains. C1-30n279: Occurrences of Pdf and Pfr have the recognisable morphology of lava plains. In several places the combination of Pdf and Pfr makes the surface strongly resembling tessera. C1-30n297: In close association with tessera there are occurrences of Pfr with gently rolling plains surface. Sometimes both tessera and Pfr deformed by graben which make the gradual transition between Pfr and Tt. C1-30n315: Pdf and Pfr occasionally look like tessera because

they are radar bright, complexly deformed, and elevated. Deformation, however, is more regular than that typical of tessera. C1-30n333: The terrain which looks to be transitional to tessera occurs where the fractures typical of Pdf are bent. This complicates the more regular pattern of the unit's deformation. C1-30n351: There is no the transitional terrain between Pdf and Pfr and tessera.

Discussion

Quasitessera, the morphology of which resembles tessera but has a simpler structural pattern, occurs within Pdf and Pfr units. Within the mapped area there is evidence that these units embay tessera and thus are younger than both tessera material and tessera-forming tectonics. It means that this tessera-like terrain represents relatively late tectonic activity in the earliest observable history of Venus. The upper stratigraphic limit of this activity, however, is at the position of Psh and Pwrl units because they are lightly deformed, mostly by wrinkle ridges. There are two important characteristics of quasitessera illustrating how the tessera-forming deformation changed through time.

1) The total area of the normal tessera is about 8% of the mapped area and the total area of quasitessera is significantly less than 1%. The typical size of the tessera-like occurrences is a few tens of km and their area is about several hundred of km2. In contrast, typical dimensions of the normal tessera massifs are about 100 by 200 km and their typical area is about 57,000 km2. The largest tessera regions are as large as a few thousand km across and have typical area about several million km2 [4) Ivanov,M.A. and Head,J.W. JGR, 101, 14861, 1996,]. This comparison shows that the typical dimensions of quasitessera are two and more orders of magnitude smaller than the typical dimensions of the fragments of normal tessera. The negligible combined area of the tessera-like terrain and small size of its occurrences suggests that even if quasitessera is the result of a hypothetical late phase of the tessera formation, the activity of this phase dropped down abruptly after the normal tessera had been formed.
2) The tessera-like terrain occurs within Pdf and Pfr units only complicating small portions of their surface. When Tt, Pdf, and Pfr occur together within any C1 the younger units usually embay tessera and show no evidence of quasitessera. The tessera-like terrain is visible only at some contacts between tessera and the younger units. Sometimes quasitessera is within self-standing occurrences either of Pdf or Pfr. This means that quasitessera terrain is neither a regular member of the morphological range from tessera to more simply deformed Pdf and Pfr, nor a regular member of the stratigraphic succession which begins from tessera. The appearance of quasitessera occasionally within either Pfd or Pfr, and not necessarily at the contact of these units with the normal tessera, suggests that there was no continuous, even dying out, phase of the formation of "new" tessera.

Conclusions

Our detailed stratigraphic mapping of a significant portion of Venus' surface showed the nature and distribution of terrain which is sharing the morphology of both tessera and other younger tectonically deformed units. Such a terrain, quasitessera, occurs as small (a few tens of km across) areas within either Pdf or Pfr and not necessarily at their contact with the normal tessera. The upper stratigraphic limit of the quasitessera formation is Psh and Pwrl plains. Such characteristics of the size and areal distribution of quasitessera and its geologic position strongly suggest that: 1) quasitessera formed occasionally and locally in the period after the normal tessera; 2) the formation of the old tessera and relatively young quasitessera is not linked by the continuous process; 3) the formation of tessera stopped relatively abruptly; 4) tessera represents an independent stratigraphic unit.

References. 1) Barsukov,V.L. et al. JGR, 91, D399, 1986, 2) Sukhanov, A. L. Tesserae In: Venus Geology, Geochemistry, and Geophysics, V.L.Barsukov, et al. eds., Univ. Arizona Press, Tucson, London, 82, 1992, 3) Bindschadler, D. L. and J. W. Head JGR, 96, 5889, 1991, 4) Ivanov, M. A. and Head, J. W. JGR, 101, 14861, 1996, 5) Crown, D. A. et al. LPSC XXV (Abstr.), 301, 1994, 6) Greeley, R. et al. LPSC XXV (Abstr.), 463, 1994, 7) Head, J. W. et al. LPSC XXV (Abstr.), 529, 1994, 8) Zimbelman, J. R. LPSC XXV (Abstr.), 1553, 1994, 9) Rosenberg, L. LPSC XXVI (Abstr.), 1185, 1995, 10) Basilevsky, A. T. and Head, J. W. EMP, 66, 285, 1995, 11) Basilevsky, A. T. and Head, J. W. Planet. Space Sci., 43, 1523, 1995, 12) Hansen, V. L. and Willis, J. J. Icarus, 123, 296, 1996 13) Basilevsky, A. T. and Head, J. W. GRL, 23, 1497, 1996, 14) Head, J. W. and Ivanov, M. A. LPSC XXVII (Abstr.), 515, 1996.

The Use of Magnetic Signatures in Identifying Shallow Intrusions on the Moon. P. A. Jackson[1], L. Wilson[1,2] and J.W. Head[2], [1]Environmental Science Division, Institute of Environmental and Biological Sciences, Lancaster University, Lancaster LA1 4YQ, U.K., [2]Department of Geological Sciences, Brown University, Providence, RI 02912, U.S.A.

Abstract: Some lunar graben (linear and arcuate rilles) may form as a result of shallow dyke intrusion, since the significantly negative buoyancy of lunar basalts in the anorthositic crust means that many dykes stall before reaching the surface [1]. Because the Moon exhibits remanent magnetism, shallow dykes are also a potential source of magnetic anomalies near the lunar surface [2]. Using a trace from the Apollo 15 sub-satellite showing magnetic field variations between (19S, 68W) and (2N, 44E) [3], all the graben near the satellite ground track were analysed using the methods of Head & Wilson [1] to determine the likelihood that they were formed by shallow intrusions. Three strong candidates were found among the thirteen examined, and others are possible.

Analysis: Mastin & Pollard [3] showed how the stress induced by a shallow intrusion would affect surface deformation and fracturing to produce graben. Head & Wilson [1] applied this analysis to two lunar graben, using the widths and depths of the graben to infer the depths to the dyke tops and the mean widths of the dykes. We used their Fig. 2b (after noting a typographic error in the strain labels) to carry out the same analysis for an additional eleven graben near the Apollo 15 sub-satellite ground track. By assuming that the horizontal extent of the outcrop of a dyke is comparable to the vertical extent of the dyke [4], a minimum source depth for the magma in the inferred dyke can be estimated from the observed graben length. For a dyke originating from the base of the crust (depth of 64 to 100 km) to stall near the surface, a driving pressure in the range 14 to 20 MPa is needed which corresponds to a dyke width of 150 to 200 m, and if the dyke originated from a strength trap in the mantle (depth or order 300 km) it would need a driving pressure of ~50 MPa, corresponding to a dyke width of 600 to 800 m [5]. Using these limits it is possible to determine if a given graben could plausibly have been formed by shallow dyke intrusion.

Results: The results of the analyses of the graben near the magnetic trace are shown in the Table below. Three strong candidates for formation due to shallow dyke intrusion are apparent, Rimae Sirsalis, Parry V and Hyginus. All three have associated volcanic features, and their inferred dyke widths and source depths are compatible with the necessary conditions. Two other possible candidates are the rilles in Alphonsus (also linked to volcanic activity) and the rille cutting the rim of Hipparchus. These and the other graben are now discussed in turn.

Rima Sirsalis has an implied minimum magma source depth of 300 km and an implied dyke width of 600 m. Thus it is possible that Rima Sirsalis formed due to a shallow intrusion of magma originating at a strength trap in the mantle.

Rima Parry V has an implied minimum source depth of 50 km and an implied dyke width of ~150 m. Thus it is plausible that Rima Parry V formed above a dyke originating at the base of the crust.

Rima Hyginus has a minimum source depth of 120 km and an implied dyke width of ~250 m. Thus it is plausible that Rima Hyginus formed due to shallow intrusion of a dyke originating just below the base of the crust.

The graben studied in Alphonsus has a minimum source depth of 25 km and an implied dyke width of.100 m, and thus appears too small to be due to shallow dyke intrusion. However, the volcanic features in Alphonsus are likely to have been fed by dykes propagated from magma intruding the brecciated zone beneath Alphonsus in association with the flooding of Mare Nubium [6], giving an effective source depth of order 20 km, consistent with our measurement.

The graben studied in Hipparchus has a minimum source depth of 37 km and an implied dyke width of.~175 m. Since the source depth is deduced from the graben length and this may not fully reflect the dyke length if the upper edge is significantly curved, this dyke too is a marginal candidate for shallow intrusion.

Rima Ariadaeus is probably a radial graben generated in response to basin formation. The inferred source depth and dyke width are too large for a dyke propagating from the base of the crust and probably too small for a dyke propagating from a strength trap in the mantle.

The other arcuate graben investigated are all thought to have been formed tectonically in

response to basin formation and loading of the maria. The likelihood that some could be the result of shallow dyke intrusion, with the resulting graben being curved due to the nature of the stress fields in crustal rocks at the edges of basins, is small, as the inferred source depths and dyke widths are not consistent with the expected behaviour of dykes

The dykes that fed the mare flood basalts must still be present in the crust;.when surface eruption ceased the surface fissure vent may have closed due to stress relaxation and been buried by lava drainback; but the shape of the dike required to deliver negatively buoyant magma to the surface will have been such as to leave a cooling crustal dyke of enormous volume [5]. Further investigation of magnetic data should help identify some of these dykes and hence locate vent sites for mare eruptions.

If the magnetic signatures in the trace we studied are indeed the result of shallow dyke intrusion, then the distance of the dike from the trace (and the dyke size) will affect the magnetic field flux ratio. We therefore plotted the flux ratio for each peak on the trace against [(distance from trace)/(graben length)], i.e. D/L in the Table for the graben associated with that peak. As this ratio increases the flux ratio would be expected to decrease, though various factors such as the orientation of the dyke, might greatly complicate the correlation.

The predicted trend of decreasing flux ratio with increasing D/L is apparent in the graph (not shown here), especially at low D/L where most of the data points are for the graben inferred to have been formed by shallow dyke intrusion. All of the points with D/L greater than ~5, which form a separate trend on the graph, are from arcuate or radial tectonic graben (which tend to have small values of L). However, there are two "tectonic" graben with very low values of D/L, the radial Rima Ariadaeus and an arcuate rille, and these must be assumed to lie by chance on the expected trend for intrusions. With some care, therefore, the flux ratio-(D/L) plot may be used to help identify graben formed by dyke intrusion. There is one major anomaly on the flux-(D/L) graph: the graben in Alphonsus with a D/L of 10 and a flux ratio of 0.38. The high flux ratio in this case is probably the result of complications from ignoring the several other graben with volcanic associations on the floor of Alphonsus.

Conclusion: Our analysis finds at least 4 probable examples of shallow intrusions with remanent magnetic signatures on the Moon and suggests that use of magnetic data can greatly enhance other methods of identifying the presence of shallow dykes.

References: [1] Head, J.W & Wilson, L. (1993) PSS 41, 719. [2] Srnka, L et al. (1979) Phys. Earth. Plan. Int. 20, 281. [3] Mastin, L.G. & Pollard, D.D. (1988) JGR 93, 13221. [4] Takeda, A (1990) JGR 95, 8471. [5] Head, J.W & Wilson, L. (1992) GCA 56, 2155. [6] Wilson, L. & Head, J.W. (1979) Proc. LPSC 10, 2861.

Table: Lat, Long of flux measurement and Flux value; Orbiter frame and feature name; Type (R = radial, C = concentric, Cr = partly in crater, V = associated volcanics); L = graben length, equal to minimum magma source depth; D = distance of graben from trace; G = graben width; T = inferred depth to dyke top; W = inferred dyke width.

Lat/Long	Flux	LO Frame	Rille Name	Type	L(km)	D(km)	G(m)	T (m)	W (m)	D/L
-15, -61	0.95	IV162H	Rima Sirsalis	R, V	300	0	3720	1200	413-534	0.0
-11, -29	0.22	IV132H	25S, 28W	C	19	450	2480	940	367-552	23.7
-11, -29	0.22	IV143H	R. Mersenius III	C	15	100	3810	1490	374-422	6.7
-11, -29	0.22	IV125H	25S, 25W	C	252	600	2880	1100	189-258	2.4
-10, -17	0.38	V38M	Rima Parry V	Cr, V	50	75	1840	680	93-171	1.5
-9, -9	0.38	IV108H	in Alphonsus	Cr, V	25	250	640	220	43-160	10.0
-7, 4	0.25	IV101H	in Hipparchus	Cr	37	60	790	280	106-343	1.6
-8, 8	0.22	III73M	Rima Hyginus	V	120	400	2010	750	194-346	3.3
-5, 14	0.15	IV90H	Rima Ariadaeus	R	165	350	3800	1490	326-367	2.1
-3, 22	0.22	IV84H	Rima Hypatia I	C	12	90	3190	1230	118-150	7.5
-2, 36	0.18	IV73H	Rima Cauchy I	C	16	400	2830	1080	142-196	25.0
-1, 38	0.25	IV73H	Rima Cauchy I	C	16	400	2830	1080	142-196	25.0
0, 44	0.17	IV65H	Fossa Messier	M	10	350	500	170	59-260	35.0